CMS PAPER HIG-14-002

DRAFT
CMS Paper

The content of this note is intended for CMS internal use and distribution only

2014/06/09
Head Id: 245278
Archive Id: 245404M
Archive Date: 2014/06/06
Archive Tag: trunk

Constraints on the Higgs boson width from off-shell production and decay to Z-boson pairs

The CMS Collaboration

Abstract

Constraints are presented on the total width of the recently discovered Higgs boson, Γ_{H}, using its relative on-shell and off-shell production and decay rates to a pair of Z bosons, where one Z boson decays to an electron or muon pair, and the other to an electron, muon, or neutrino pair. The analysis is based on the data collected by the CMS experiment at the LHC in 2011 and 2012, corresponding to integrated luminosities of $5.1\,\mathrm{fb}^{-1}$ at a centre-of-mass energy $\sqrt{s} = 7\,\mathrm{TeV}$ and $19.7\,\mathrm{fb}^{-1}$ at $\sqrt{s} = 8\,\mathrm{TeV}$. A simultaneous maximum likelihood fit to the measured kinematic distributions near the resonance peak and above the Z-boson pair production threshold leads to an upper limit on the Higgs boson width of $\Gamma_{\mathrm{H}} < 22\,\mathrm{MeV}$ at a 95% confidence level, which is 5.4 times the expected value in the standard model at the measured mass of $m_{\mathrm{H}} = 125.6\,\mathrm{GeV}$.

This box is only visible in draft mode. Please make sure the values below make sense.

PDFAuthor:	Claude Charlot, Roberto Covarelli, Jian Wang
PDFTitle:	Constraints on the Higgs boson width from off-shell production and decay to Z-boson pairs
PDFSubject:	CMS
PDFKeywords:	CMS, physics, higgs, diboson, properties

Please also verify that the abstract does not use any user defined symbols

DRAFT

The discovery of a new boson consistent with the standard model (SM) Higgs boson by the ATLAS and CMS Collaborations was recently reported [1–3]. The mass of the new boson (m_{H}) was measured to be near 125 GeV, and the spin-parity properties were further studied by both experiments, favouring the scalar, $\mathrm{J^{PC}} = 0^{++}$, hypothesis [4–7]. The measurements were found to be consistent with a single narrow resonance, and an upper limit of 3.4 GeV at a 95% confidence level (CL) on its decay width (Γ_{H}) was reported by the CMS experiment in the four-lepton decay channel [7]. A direct width measurement at the resonance peak is limited by experimental resolution, and is only sensitive to values far larger than the expected width of around 4 MeV for the SM Higgs boson [8, 9].

It was recently proposed [10] to constrain the Higgs boson width using its off-shell production and decay to two Z bosons away from the resonance peak [11]. In the dominant gluon fusion production mode the off-shell production cross section is known to be sizable. This arises from an enhancement in the decay amplitude from the vicinity of the Z-boson pair production threshold. A further enhancement comes, in gluon fusion production, from the top-quark pair production threshold. The zero-width approximation is inadequate and the ratio of the off-shell cross section above $2m_{\mathrm{Z}}$ to the on-shell signal is of the order of 8% [11, 12]. Further developments to the measurement of the Higgs boson width were proposed in Refs. [13, 14].

The gluon fusion production cross section depends on Γ_{H} through the Higgs boson propagator

$$\frac{\mathrm{d}\sigma_{\mathrm{gg\to H\to ZZ}}}{\mathrm{d}m^2_{\mathrm{ZZ}}} \sim \frac{g^2_{\mathrm{ggH}} g^2_{\mathrm{HZZ}}}{(m^2_{\mathrm{ZZ}} - m^2_{\mathrm{H}})^2 + m^2_{\mathrm{H}}\Gamma^2_{\mathrm{H}}}, \tag{1}$$

where g_{ggH} and g_{HZZ} are the couplings of the Higgs boson to gluons and Z bosons, respectively. Integrating either in a small region around m_{H}, or above the mass threshold $m_{\mathrm{ZZ}} > 2m_{\mathrm{Z}}$, where $(m_{\mathrm{ZZ}} - m_{\mathrm{H}}) \gg \Gamma_{\mathrm{H}}$, the cross sections are, respectively,

$$\sigma^{\text{on-shell}}_{\mathrm{gg\to H\to ZZ^*}} \sim \frac{g^2_{\mathrm{ggH}} g^2_{\mathrm{HZZ}}}{m_{\mathrm{H}}\Gamma_{\mathrm{H}}} \quad \text{and} \quad \sigma^{\text{off-shell}}_{\mathrm{gg\to H^*\to ZZ}} \sim \frac{g^2_{\mathrm{ggH}} g^2_{\mathrm{HZZ}}}{(2m_{\mathrm{Z}})^2}. \tag{2}$$

From Eq. (2), it is clear that a measurement of the relative off-shell and on-shell production in the $\mathrm{H} \to \mathrm{ZZ}$ channel provides direct information on Γ_{H}, as long as the coupling ratios remain unchanged, i.e. the gluon fusion production is dominated by the top-quark loop and there are no new particles contributing. In particular, the on-shell production cross section is unchanged under a common scaling of the squared product of the couplings and of the total width Γ_{H}, while the off-shell production cross section increases linearly with this scaling factor.

The dominant contribution for the production of a pair of Z bosons comes from the quark-initiated process, $\mathrm{q\bar{q}} \to \mathrm{ZZ}$, the diagram for which is displayed in Fig. 1(left). The gluon-induced diboson production involves the $\mathrm{gg} \to \mathrm{ZZ}$ continuum background production from the box diagrams, as illustrated in Fig. 1(center). An example of the signal production diagram is shown in Fig. 1(right). The interference between the two gluon-induced contributions is significant at high m_{ZZ} [15], and is taken into account in the analysis of the off-shell signal.

Vector boson fusion (VBF) production, which contributes at the level of about 7% to the on-shell cross section, is expected to increase above $2m_{\mathrm{Z}}$. The above formalism describing the ratio of off-shell and on-shell cross sections is applicable to the VBF production mode. In this analysis we constrain the fraction of VBF production using the properties of the events in the on-shell region. The other main Higgs boson production mechanisms, $\mathrm{t\bar{t}H}$ and VH (V=Z,W), which contribute at the level of about 5% to the on-shell signal, are not expected to produce a significant off-shell contribution as they are suppressed at high mass [8, 9]. They are therefore neglected in the off-shell analysis.

DRAFT

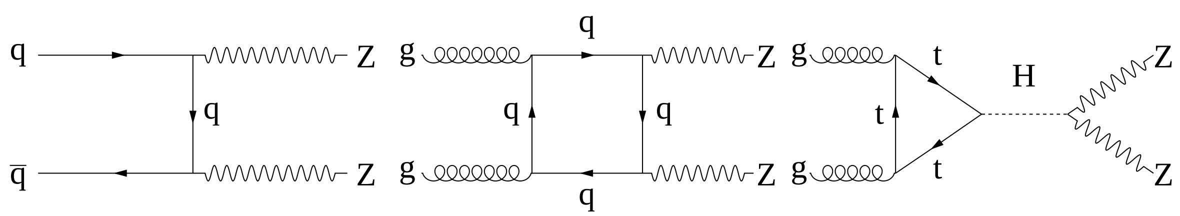

Figure 1: Lowest order contributions to the main ZZ production processes: (left) quark-initiated production, $q\overline{q} \to ZZ$, (center) gg continuum background production, $gg \to ZZ$, and (right) Higgs-mediated gg production, $gg \to H \to ZZ$, the signal.

In this Letter, we present constraints on the Higgs boson width using its off-shell production and decay to Z-boson pairs, in the final states where one Z boson decays to an electron or a muon pair and the other to either an electron or a muon pair, $H \to ZZ \to 4\ell$ (4ℓ channel), or a pair of neutrinos, $H \to ZZ \to 2\ell 2\nu$ ($2\ell 2\nu$ channel). Relying on the observed Higgs boson signal in the resonance peak region [7], the simultaneous measurement of the signal in the high-mass region leads to constraints on the Higgs boson width Γ_H in the 4ℓ decay channel. The $2\ell 2\nu$ decay channel, which benefits from a higher branching fraction [16, 17], is used in the high-mass region to further increase the sensitivity to the Higgs boson width. The analysis is performed for the tree-level HVV coupling of a scalar Higgs boson, consistent with our observations [4, 7], and implications for the anomalous HVV interactions are discussed. The Higgs boson mass is set to the measured value in the 4ℓ decay channel of $m_H = 125.6\,\text{GeV}$ [7] and the Higgs boson width is set to the corresponding expected value in the SM of $\Gamma_H^{SM} = 4.15\,\text{MeV}$ [8, 9].

The measurement is based on pp collision data collected with the CMS detector at the LHC in 2011, corresponding to an integrated luminosity of $5.1\,\text{fb}^{-1}$ at the center-of-mass energy of $\sqrt{s} = 7\,\text{TeV}$ (4ℓ channel), and in 2012, corresponding to an integrated luminosity of $19.7\,\text{fb}^{-1}$ at $\sqrt{s} = 8\,\text{TeV}$ (4ℓ and $2\ell 2\nu$ channels). The CMS detector, described in detail elsewhere [18], provides excellent resolution for the measurement of electron and muon transverse momenta (p_T) over a wide range. The signal candidates are selected using well-identified and isolated prompt leptons. The online selection and event reconstruction are described elsewhere [2, 3, 7, 16]. The analysis presented here is based on the same event selection as used in Refs. [7, 16].

The analysis in the 4ℓ channel uses the four-lepton invariant mass distribution as well as a matrix element likelihood discriminant to separate the ZZ components originating from gluon- and quark-initiated processes. We define the on-shell signal region as $105.6 < m_{4\ell} < 140.6\,\text{GeV}$ and the off-shell signal region as $m_{4\ell} > 220\,\text{GeV}$. The analysis in the $2\ell 2\nu$ channel relies on the transverse mass distribution m_T,

$$m_T^2 = \left[\sqrt{{p_{T,2\ell}}^2 + {m_{2\ell}}^2} + \sqrt{{E_T^{miss}}^2 + {m_{2\ell}}^2} \right]^2 - \left[\vec{p}_{T,2\ell} + \vec{E}_T^{miss} \right]^2, \tag{3}$$

where $p_{T,2\ell}$ and $m_{2\ell}$ are the measured transverse momentum and invariant mass of the dilepton system, respectively. The missing transverse energy, E_T^{miss}, is defined as the magnitude of the transverse momentum imbalance evaluated as the negative of the vectorial sum of transverse momenta of all the reconstructed particles in the event. In the $2\ell 2\nu$ channel, the off-shell signal region is defined as $m_T > 180\,\text{GeV}$. The choice of the off-shell regions in both channels is done prior to looking at the data, based on the expected sensitivity.

Simulated Monte Carlo (MC) samples of $gg \to 4\ell$ and $gg \to 2\ell 2\nu$ events are generated at leading order (LO) in perturbative quantum chromodynamics (QCD), including the Higgs boson signal, the continuum background, and the interference contributions using recent versions of two different MC generators, GG2VV 3.1.5 [11, 19] and MCFM 6.7 [20], in order to cross-check theoretical inputs. The QCD renormalization and factorization scales are set to $m_{ZZ}/2$ (dynamic scales) and MSTW2008 LO parton distribution functions (PDFs) [21] are used. Higher-order QCD corrections for the gluon fusion signal process are known to an accuracy of next-to-next-to-leading order (NNLO) and next-to-next-to-leading logarithms for the total cross section [8, 9] and to NNLO as a function of m_{ZZ} [14]. These correction factors to the LO cross section (K factors) are typically in the range of 2.0 to 2.5. After the application of the m_{ZZ}-dependent K factors, the event yield is normalized to the cross section from Refs. [8, 9]. For the gg $\to$ ZZ continuum background, although no exact calculation exists beyond LO, it has been recently shown [22] that the soft collinear approximation is able to describe the background cross section and therefore the interference term at NNLO. Following this calculation, we assign to the LO background cross section (and, consequently, to the interference contribution) a K factor equal to that used for the signal [14]. The limited theoretical knowledge of the background K factor at NNLO is taken into account by including an additional systematic uncertainty, the impact of which on the measurement is nevertheless small.

Vector boson fusion events are generated with PHANTOM [23]. Off-shell and interference effects with the nonresonant production are included at LO in these simulations. The event yield is normalized to the cross section at NNLO QCD and next-to-leading order (NLO) electroweak (EW) [8, 9] accuracy, with a normalization factor shown to be independent of m_{ZZ}.

In order to parameterize and validate the distributions of all the components for both gluon fusion and VBF processes, specific simulated samples are also produced that describe only the signal or the continuum background, as well as several scenarios with scaled couplings and width. For the on-shell analysis, signal events are generated either with POWHEG [24–27] production at NLO in QCD and JHUGEN [28, 29] decay (gluon fusion and VBF), or with PYTHIA 6.4 [30] (VH and $t\bar{t}$H production).

In both the 4ℓ and $2\ell2\nu$ channels the dominant background is $q\bar{q} \to$ ZZ. We assume SM production rates for this background, the contribution of which is evaluated by POWHEG simulation at NLO in QCD [31]. Next-to-leading order EW calculations [32, 33], which predict negative and m_{ZZ}-dependent corrections to the $q\bar{q} \to$ ZZ process for on-shell Z-boson pairs, are taken into account.

All simulated events undergo parton showering and hadronization using PYTHIA. As is done in Ref. [7] for LO samples, the parton showering settings are tuned to approximately reproduce the ZZ p_T spectrum predicted at NNLO for the Higgs boson production [34]. Generated events are then processed with the detailed CMS detector simulation based on GEANT4 [35, 36], and reconstructed using the same algorithms as used for the observed events.

The final state in the 4ℓ channel is characterized by four well-identified and isolated leptons forming two pairs of opposite-sign and same-flavour leptons consistent with two Z bosons. This channel benefits from a precise reconstruction of all final state leptons and from a very low instrumental background. The event selection and the reducible background evaluation are performed following the methods described in Ref. [7]. After the selection, the 4ℓ data sample is dominated by the quark-initiated $q\bar{q} \to ZZ \to 4\ell$ ($q\bar{q} \to 4\ell$) and gg $\to 4\ell$ productions.

Figure 2 presents the measured $m_{4\ell}$ distribution over the full mass range, $m_{4\ell} > 100$ GeV, together with the expected SM contributions. The gg $\to 4\ell$ contribution is clearly visible in the on-shell signal region and at the Z-boson pair production threshold, above the $q\bar{q} \to 4\ell$ background. The observed distribution is consistent with the expectation from SM processes. We observe 223 events in the off-shell signal region, while we expect 217.6 ± 9.5 from SM processes, including the SM Higgs boson signal.

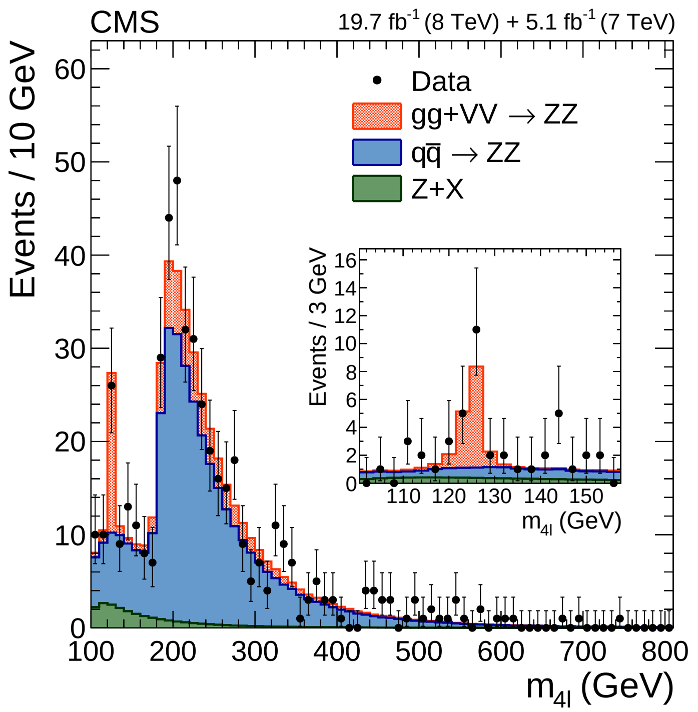

Figure 2: Distribution of the four-lepton invariant mass in the range $100 < m_{4\ell} < 800\,\text{GeV}$. Points represent the data, filled histograms the expected contributions from the reducible (Z+X) and $q\bar{q}$ backgrounds, and from the sum of the gluon fusion (gg) and vector boson fusion (VV) processes, including the Higgs boson mediated contributions. The inset shows the distribution in the low mass region after a selection requirement on the MELA likelihood discriminant $\mathcal{D}^{\text{kin}}_{\text{bkg}} > 0.5$ [7]. In this region, the contribution of the $t\bar{t}$H and VH production processes is added to the dominant gluon fusion and VBF contributions.

In order to enhance the sensitivity to the gg production in the off-shell region, a likelihood discriminant $\mathcal{D}_{gg}$ is used, which characterizes the event topology in the 4ℓ centre-of-mass frame using the observables $(m_{Z_1}, m_{Z_2}, \vec{\Omega})$ for a given value of $m_{4\ell}$, where $\vec{\Omega}$ denotes the five angles defined in Ref. [28]. The discriminant is built from the probabilities $\mathcal{P}^{gg}_{\text{tot}}$ and $\mathcal{P}^{q\bar{q}}_{\text{bkg}}$ for an event to originate from either the $gg \to 4\ell$ or the $q\bar{q} \to 4\ell$ process. We use the matrix element likelihood approach (MELA) [2, 29] for the probability computation using the MCFM matrix elements for both $gg \to 4\ell$ and $q\bar{q} \to 4\ell$ processes. The probability $\mathcal{P}^{gg}_{\text{tot}}$ for the $gg \to 4\ell$ process includes the signal ($\mathcal{P}^{gg}_{\text{sig}}$), the background ($\mathcal{P}^{gg}_{\text{bkg}}$), and their interference ($\mathcal{P}^{gg}_{\text{int}}$), as introduced for the discriminant computation in Ref. [37]. The discriminant is defined as

$$\mathcal{D}_{gg} = \frac{\mathcal{P}^{gg}_{\text{tot}}}{\mathcal{P}^{gg}_{\text{tot}} + \mathcal{P}^{q\bar{q}}_{\text{bkg}}} = \left[1 + \frac{\mathcal{P}^{q\bar{q}}_{\text{bkg}}}{a \times \mathcal{P}^{gg}_{\text{sig}} + \sqrt{a} \times \mathcal{P}^{gg}_{\text{int}} + \mathcal{P}^{gg}_{\text{bkg}}}\right]^{-1}, \quad (4)$$

where the parameter a is the strength of the unknown anomalous gg contribution with respect to the expected SM contribution ($a = 1$). We set $a = 10$ in the definition of $\mathcal{D}_{gg}$ according to the expected sensitivity. Studies show that the expected sensitivity does not change substantially when a is varied up or down by a factor of 2. It should be stressed that fixing the parameter a

to a given value only affects the sensitivity of the analysis. To suppress the dominant $q\bar{q} \to 4\ell$ background in the on-shell region, the analysis also employs a MELA likelihood discriminant $\mathcal{D}_{\mathrm{bkg}}^{\mathrm{kin}}$ based on the JHUGEN and MCFM matrix element calculations for the signal and the background, as illustrated by the inset in Fig. 2 and used in Ref. [7].

As an illustration, Fig. 3(top) presents the 4ℓ invariant mass distribution for the off-shell signal region ($m_{4\ell} > 220\,\mathrm{GeV}$) and for $\mathcal{D}_{\mathrm{gg}} > 0.65$. The expected contributions from the $q\bar{q} \to 4\ell$ and reducible backgrounds, as well as for the total gluon fusion (gg) and vector boson fusion (VV) contributions, including the Higgs boson signal, are shown. The distribution of the likelihood discriminant $\mathcal{D}_{\mathrm{gg}}$ for $m_{4\ell} > 330\,\mathrm{GeV}$ is shown in Fig. 3(bottom), together with the expected contributions from the SM. The expected $m_{4\ell}$ and $\mathcal{D}_{\mathrm{gg}}$ distributions for the sum of all the processes, with a Higgs boson width $\Gamma_{\mathrm{H}} = 10 \times \Gamma_{\mathrm{H}}^{\mathrm{SM}}$ and a relative cross section with respect to the SM cross section equal to unity in both gluon fusion and VBF production modes ($\mu = \mu_{\mathrm{ggH}} = \mu_{\mathrm{VBF}} = 1$), are also presented, showing the enhancement arising from the scaling of the squared product of the couplings. The expected and observed event yields in the off-shell gg-enriched region defined by $m_{4\ell} \geq 330\,\mathrm{GeV}$ and $\mathcal{D}_{\mathrm{gg}} > 0.65$ are reported in Table 1.

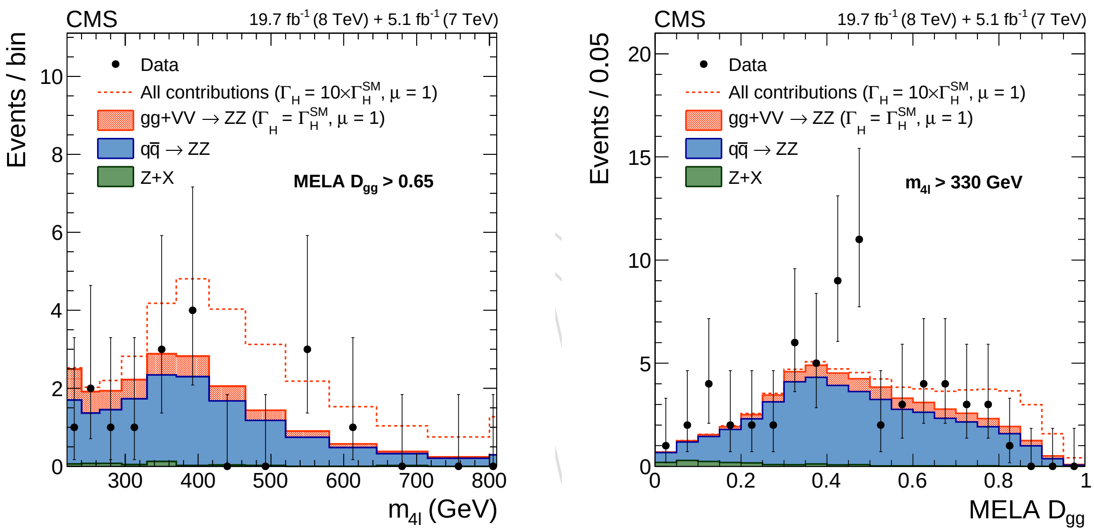

Figure 3: Distributions of (top) the four-lepton invariant mass after a selection requirement on the MELA likelihood discriminant $\mathcal{D}_{\mathrm{gg}} > 0.65$, and (bottom) the $\mathcal{D}_{\mathrm{gg}}$ likelihood discriminant for $m_{4\ell} > 330\,\mathrm{GeV}$ in the 4ℓ channel. Points represent the data, filled histograms the expected contributions from the reducible (Z+X) and $q\bar{q}$ backgrounds, and from the gluon fusion (gg) and vector boson fusion (VV) SM processes (including the Higgs boson mediated contributions). The dashed line corresponds to the total expected yield for a Higgs boson width and a squared product of the couplings scaled by a factor 10 with respect to their SM values. In the top plot, the bin size varies from 20 to 85 GeV and the last bin includes all entries with masses above 800 GeV.

The $2\ell 2\nu$ analysis is performed on the 8 TeV data set only. The final state in the $2\ell 2\nu$ channel is characterized by two oppositely-charged leptons of the same flavour compatible with a Z boson, together with a large $E_{\mathrm{T}}^{\mathrm{miss}}$ from the undetectable neutrinos. We require $E_{\mathrm{T}}^{\mathrm{miss}} > 80\,\mathrm{GeV}$. The event selection and background estimation is performed as described in Ref. [16], with the exception that the jet categories defined in Ref. [16] are here grouped into a single category, i.e. the analysis is performed in an inclusive way. The m_{T} distribution in the off-shell signal region ($m_{\mathrm{T}} > 180\,\mathrm{GeV}$) is shown in Fig. 4. The expected and observed event yields in a gg-enriched region defined by $m_{\mathrm{T}} > 350\,\mathrm{GeV}$ and $E_{\mathrm{T}}^{\mathrm{miss}} > 100\,\mathrm{GeV}$ are reported in Table 1.

Table 1: Expected and observed numbers of events in the 4ℓ and $2\ell2\nu$ channels in gg-enriched regions, defined by $m_{4\ell} \geq 330\,\mathrm{GeV}$ and $\mathcal{D}_{\mathrm{gg}} > 0.65$ (4ℓ), and by $m_{\mathrm{T}} > 350\,\mathrm{GeV}$ and $E_{\mathrm{T}}^{\mathrm{miss}} > 100\,\mathrm{GeV}$ ($2\ell2\nu$). The numbers of expected events are given separately for the gg and VBF processes, and for a SM Higgs boson ($\Gamma_{\mathrm{H}} = \Gamma_{\mathrm{H}}^{\mathrm{SM}}$) and a Higgs boson width and squared product of the couplings scaled by a factor 10 with respect to their SM values. The unphysical expected contributions for the signal and background components are also reported separately, for the gg and VBF processes. For both processes, the sum of the signal and background components differs from the total due to the negative interferences. The quoted uncertainties include only the systematic sources.

		4ℓ	$2\ell2\nu$
(a)	Total gg ($\Gamma_{\mathrm{H}} = \Gamma_{\mathrm{H}}^{\mathrm{SM}}$)	1.8 ± 0.3	9.6 ± 1.5
	gg Signal component ($\Gamma_{\mathrm{H}} = \Gamma_{\mathrm{H}}^{\mathrm{SM}}$)	1.3 ± 0.2	4.7 ± 0.6
	gg Background component	2.3 ± 0.4	10.8 ± 1.7
(b)	Total gg ($\Gamma_{\mathrm{H}} = 10 \times \Gamma_{\mathrm{H}}^{\mathrm{SM}}$)	9.9 ± 1.2	39.8 ± 5.2
(c)	Total VBF ($\Gamma_{\mathrm{H}} = \Gamma_{\mathrm{H}}^{\mathrm{SM}}$)	0.23 ± 0.01	0.90 ± 0.05
	VBF signal component ($\Gamma_{\mathrm{H}} = \Gamma_{\mathrm{H}}^{\mathrm{SM}}$)	0.11 ± 0.01	0.32 ± 0.02
	VBF background component	0.35 ± 0.02	1.22 ± 0.07
(d)	Total VBF ($\Gamma_{\mathrm{H}} = 10 \times \Gamma_{\mathrm{H}}^{\mathrm{SM}}$)	0.77 ± 0.04	2.40 ± 0.14
(e)	$\mathrm{q\bar{q}}$ background	9.3 ± 0.7	47.6 ± 4.0
(f)	Other backgrounds	0.05 ± 0.02	35.1 ± 4.2
(a+c+e+f)	Total expected ($\Gamma_{\mathrm{H}} = \Gamma_{\mathrm{H}}^{\mathrm{SM}}$)	11.4 ± 0.8	93.2 ± 6.0
(b+d+e+f)	Total expected ($\Gamma_{\mathrm{H}} = 10 \times \Gamma_{\mathrm{H}}^{\mathrm{SM}}$)	20.1 ± 1.4	124.9 ± 7.8
	Observed	11	91

Systematic uncertainties comprise experimental uncertainties on the signal efficiency and background yield evaluation, as well as uncertainties on the signal and background from theoretical predictions. Since the measurement is performed in wide m_{ZZ} regions, there are sources of systematic uncertainties that only affect the total normalization and others that affect both the normalization and the shape of the observables used in this analysis. In the 4ℓ final state, only the latter type of systematic uncertainty affects the measurement of Γ_{H}, since normalization uncertainties change the on-shell and off-shell yields by the same amount.

Among the signal uncertainties, experimental systematic uncertainties are evaluated from observed events for the trigger efficiency (1.5%), and combined object reconstruction, identification and isolation efficiencies (3–4% for muons, 5–11% for electrons) [7]. In the $2\ell2\nu$ final state, the effects of the lepton momentum scale (1–2%) and jet energy scale (1%) are taken into account and propagated to the evaluation of $E_{\mathrm{T}}^{\mathrm{miss}}$. The uncertainty in the b-jet veto (1–3%) is estimated from simulation using correction factors for the b-tagging and b-misidentification efficiencies as measured from the dijet and $\mathrm{t\bar{t}}$ decay control samples [38].

Theoretical uncertainties from QCD scales in the $\mathrm{q\bar{q}}$ background contribution are within 4–10% depending on m_{ZZ} [7]. An additional uncertainty of 2–6% is included to account for missing higher order contributions with respect to a full NLO QCD and NLO EW evaluation. The systematic uncertainty in the normalization of the reducible backgrounds is evaluated following the methods described in Refs. [7, 16]. In the $2\ell2\nu$ channel, for which these contributions are not negligible at high mass, the estimation from control samples for the Z+jets and for the sum of the $\mathrm{t\bar{t}}$, tW and WW contributions leads to uncertainties of 25% and 15% in the respective background yields. Theoretical uncertainties in the high mass contribution from the gluon-

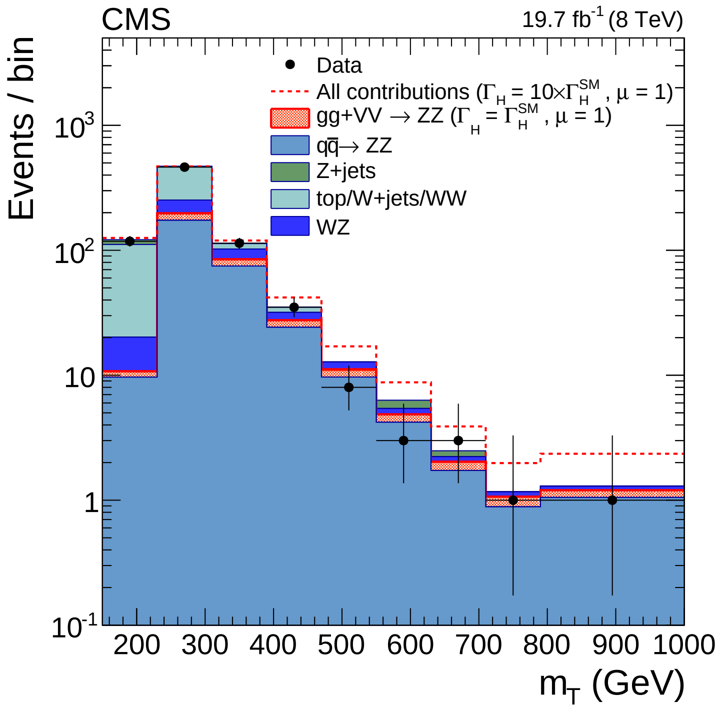

Figure 4: Distribution of the transverse mass in the $2\ell 2\nu$ channel. Points represent the data, filled histograms the expected contributions from the backgrounds, and from the gluon fusion (gg) and vector boson fusion (VV) SM processes (including the Higgs-mediated contributions). The dashed line corresponds to the total expected yield for a Higgs boson width and a squared product of the couplings scaled by a factor 10 with respect to their SM values. The bin size varies from 80 to 210 GeV and the last bin includes all entries with transverse masses above 1 TeV.

induced processes, which affect both the normalization and the shape, are especially important in this analysis (in particular for the signal and interference contributions that are scaled by large factors). However, these uncertainties partially cancel when measuring simultaneously the yield from the same process in the on-shell signal region. The remaining m_{ZZ}-dependent uncertainties in the QCD renormalization and factorization scales are derived using the K factor variations from Ref. [14], corresponding to a factor of two up or down from the nominal $m_{ZZ}/2$ values, and amount to 2–4%. For the gg $\rightarrow$ ZZ continuum background production, we assign a 10% additional uncertainty on the K factor, following Ref. [22] and taking into account the different mass ranges and selections on the specific final state. This uncertainty also affects the interference with the signal. The PDF uncertainties are estimated following Refs. [39, 40] by changing the NLO PDF set from MSTW2008 to CT10 [41] and NNPDF2.1 [42], and the residual contribution is about 1%. For the VBF processes, no significant m_{ZZ}-dependence is found regarding the QCD scales and PDF uncertainties, which are in general much smaller than for the gluon fusion processes [8, 9]. In the $2\ell 2\nu$ final state, additional uncertainties on the yield arising from the theoretical description of the parton shower and underlying event are taken into account (6%).

We perform a simultaneous unbinned maximum likelihood fit of a signal-plus-background model to the measured distributions in the 4ℓ and $2\ell 2\nu$ channels. In the 4ℓ channel the analysis is performed in the on-shell and off-shell signal regions defined above. In the on-shell region, a three-dimensional distribution $\vec{x} = (m_{4\ell}, \mathcal{D}_{\mathrm{bkg}}^{\mathrm{kin}}, p_{\mathrm{T}}^{4\ell}$ or $\mathcal{D}_{\mathrm{jet}})$ is analyzed, following the methodology described in Ref. [7], where the quantity $\mathcal{D}_{\mathrm{jet}}$ is a discriminant used to separate VBF from gluon fusion production. In the off-shell region, a two-dimensional distribution $\vec{x} = (m_{4\ell}, \mathcal{D}_{\mathrm{gg}})$ is analyzed. In the $2\ell 2\nu$ channel, only the off-shell Higgs boson production is analyzed, using the $\vec{x} = m_{\mathrm{T}}$ distribution.

The probability distribution functions are built using the full detector simulation or data control regions, and are defined for the signal, the background, or the interference between the two contributions, $\mathcal{P}_{\mathrm{sig}}$, $\mathcal{P}_{\mathrm{bkg}}$, or $\mathcal{P}_{\mathrm{int}}$, respectively, as a function of the observables $\vec{x}$ discussed above. Several production mechanisms are considered for the signal and the background, such as gluon fusion (gg), VBF, and quark-antiquark annihilation ($\mathrm{q\overline{q}}$). The total probability distribution function for the off-shell region includes the interference of two contributions in each production process:

$$\begin{aligned}\mathcal{P}_{\mathrm{tot}}^{\text{off-shell}}(\vec{x}) = &\left[\mu_{\mathrm{ggH}} \times (\Gamma_{\mathrm{H}}/\Gamma_0) \times \mathcal{P}_{\mathrm{sig}}^{\mathrm{gg}}(\vec{x}) + \sqrt{\mu_{\mathrm{ggH}} \times (\Gamma_{\mathrm{H}}/\Gamma_0)} \times \mathcal{P}_{\mathrm{int}}^{\mathrm{gg}}(\vec{x}) + \mathcal{P}_{\mathrm{bkg}}^{\mathrm{gg}}(\vec{x})\right] \\ &+ \left[\mu_{\mathrm{VBF}} \times (\Gamma_{\mathrm{H}}/\Gamma_0) \times \mathcal{P}_{\mathrm{sig}}^{\mathrm{VBF}}(\vec{x}) + \sqrt{\mu_{\mathrm{VBF}} \times (\Gamma_{\mathrm{H}}/\Gamma_0)} \times \mathcal{P}_{\mathrm{int}}^{\mathrm{VBF}}(\vec{x}) + \mathcal{P}_{\mathrm{bkg}}^{\mathrm{VBF}}(\vec{x})\right] \\ &+ \mathcal{P}_{\mathrm{bkg}}^{\mathrm{q\overline{q}}}(\vec{x}) + \ldots\end{aligned} \tag{5}$$

The list of background processes is extended beyond those quoted depending on the final state (Z+X, top, W+jets, WW, WZ). The parameters μ_{ggH} and μ_{VBF} are the scale factors which modify the signal strength with respect to the reference parameterization in each production mechanism independently. The parameter $(\Gamma_{\mathrm{H}}/\Gamma_0)$ is the scale factor which modifies the observed width with respect to the Γ_0 value used in the reference parameterization.

In the on-shell region, the parameterization includes the small contribution of the $\mathrm{t\bar{t}H}$ and VH Higgs boson production mechanisms, which are related to the gluon fusion and VBF processes, respectively, because either the quark or the vector boson coupling to the Higgs boson is in common among those processes. Interference effects are negligible in the on-shell region. The total probability distribution function for the on-shell region is written as

$$\begin{aligned}\mathcal{P}_{\mathrm{tot}}^{\text{on-shell}}(\vec{x}) = &\mu_{\mathrm{ggH}} \times \left[\mathcal{P}_{\mathrm{sig}}^{\mathrm{gg}}(\vec{x}) + \mathcal{P}_{\mathrm{sig}}^{\mathrm{t\bar{t}H}}(\vec{x})\right] + \mu_{\mathrm{VBF}} \times \left[\mathcal{P}_{\mathrm{sig}}^{\mathrm{VBF}}(\vec{x}) + \mathcal{P}_{\mathrm{sig}}^{\mathrm{VH}}(\vec{x})\right] \\ &+ \mathcal{P}_{\mathrm{bkg}}^{\mathrm{q\overline{q}}}(\vec{x}) + \mathcal{P}_{\mathrm{bkg}}^{\mathrm{gg}}(\vec{x}) + \ldots\end{aligned} \tag{6}$$

The above parameterizations in Eqs. (5, 6) are performed for the tree-level HVV coupling of a scalar Higgs boson, consistent with our observations [4, 7]. We find that the presence of anomalous couplings in the HVV interaction would lead to enhanced off-shell production and a more stringent constraint on the width. It is evident that the parameterization in Eq. (5) relies on the modeling of the gluon fusion production with the dominant top-quark loop, therefore no possible new particles are considered in the loop. Further discussion can also be found in Refs. [43–45].

The three parameters Γ_{H}, μ_{ggH}, and μ_{VBF} are left unconstrained in the fit. The μ_{ggH} and μ_{VBF} fitted values are found to be almost identical to those obtained in Ref. [7]. Systematic uncertainties are included as nuisance parameters and are treated according to the frequentist paradigm [46]. The shapes and normalizations of the signal and of each background component are allowed to vary within their uncertainties, and the correlations in the sources of systematic uncertainty are taken into account.

The fit results are shown in Fig. 5 as scans of the negative log-likelihood, $-2\Delta\ln\mathcal{L}$, as a function of Γ_{H}. Combining the two channels a limit is observed (expected) on the total width of $\Gamma_{\mathrm{H}} <$

DRAFT

22 MeV (33 MeV) at a 95% CL, which is 5.4 (8.0) times the expected value in the SM. The best fit value and 68% CL interval correspond to $\Gamma_{\mathrm{H}} = 1.8^{+7.7}_{-1.8}$ MeV. The result of the 4ℓ analysis alone is an observed (expected) limit of $\Gamma_{\mathrm{H}} < 33$ MeV (42 MeV) at a 95% CL, which is 8.0 (10.1) times the SM value, and the result of the analysis combining the 4ℓ on-shell and $2\ell 2\nu$ off-shell regions is $\Gamma_{\mathrm{H}} < 33$ MeV (44 MeV) at a 95% CL, which is 8.1 (10.6) times the SM value. The best fit values and 68% CL intervals are $\Gamma_{\mathrm{H}} = 1.9^{+11.7}_{-1.9}$ MeV and $\Gamma_{\mathrm{H}} = 1.8^{+12.4}_{-1.8}$ MeV for the 4ℓ analysis and for the analysis combining the 4ℓ on-shell and $2\ell 2\nu$ off-shell regions, respectively.

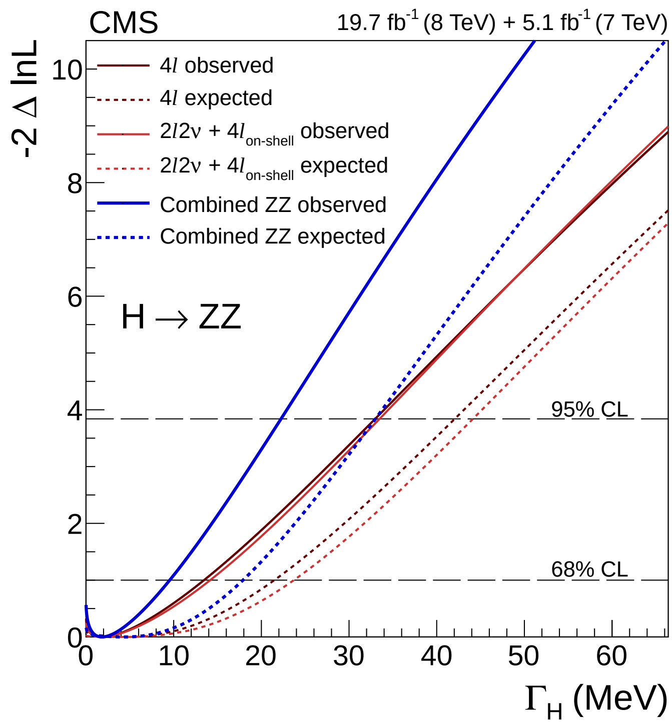

Figure 5: Scan of the negative log-likelihood, $-2\Delta \ln \mathcal{L}$, as a function of Γ_{H} for the combined fit of the 4ℓ and $2\ell 2\nu$ channels (blue thick lines), for the 4ℓ channel alone in the off-shell and on-shell regions (dark red lines), and for the $2\ell 2\nu$ channel in the off-shell region and 4ℓ channel in the on-shell region (light red lines). The solid lines represent the observed values, the dotted lines the expected values.

The expected limit for the two channels combined without including the systematic uncertainties is $\Gamma_{\mathrm{H}} < 28$ MeV at a 95% CL. The effect of systematic uncertainties is driven by the $2\ell 2\nu$ channel with larger experimental uncertainties in signal efficiencies and background estimation from control samples in data, while the result in the 4ℓ channel is largely dominated by the statistical uncertainty.

The statistical compatibility of the observed results with the expectation under the SM hypothesis corresponds to a p-value of 0.24. The statistical coverage of the results obtained in the likelihood scan has also been tested with the Feldman–Cousins approach [47] for the combined analysis leading to consistent although slightly tighter constraints. The analysis in the 4ℓ channel has also been performed in a one-dimensional fit using either $m_{4\ell}$ or $\mathcal{D}_{\mathrm{gg}}$ and consistent results are found. The expected limit without using the MELA likelihood discriminant $\mathcal{D}_{\mathrm{gg}}$ is 40% larger in the 4ℓ channel.

In summary, we have presented constraints on the total Higgs boson width using its relative on-shell and off-shell production and decay rates to four leptons or two leptons and two neutrinos. The analysis is based on the 2011 and 2012 data sets corresponding to integrated luminosities of 5.1 fb^{-1} at $\sqrt{s} = 7\,\mathrm{TeV}$ and 19.7 fb^{-1} at $\sqrt{s} = 8\,\mathrm{TeV}$. The four-lepton analysis uses the measured invariant mass distribution near the peak and above the Z-boson pair production threshold, as well as a likelihood discriminant to separate the gluon fusion ZZ production from the $\mathrm{q\overline{q}} \to \mathrm{ZZ}$ background, while the two-lepton plus two-neutrino off-shell analysis relies on the transverse mass distribution. The presented analysis determines the independent contributions of the gluon fusion and VBF production mechanisms from the data in the on-shell region. It relies nevertheless on the knowledge of the coupling ratios between the off-shell and on-shell production, i.e. the dominance of the top quark loop in the gluon fusion production mechanism and the absence of new particle contribution in the loop. The presence of anomalous couplings in the HVV interaction would lead to enhanced off-shell production and would make our constraint tighter. The combined fit of the 4ℓ and $2\ell 2\nu$ channels leads to an upper limit on the Higgs boson width of $\Gamma_{\mathrm{H}} < 22\,\mathrm{MeV}$ at a 95% confidence level, which is 5.4 times the expected width of the SM Higgs boson. This result improves by more than two orders of magnitude upon previous experimental constraints on the new boson decay width from the direct measurement at the resonance peak.

We wish to thank our theoretician colleagues and in particular Fabrizio Caola for providing the theoretical uncertainty in the $\mathrm{gg} \to \mathrm{ZZ}$ background K factor, Tobias Kasprzik for providing the numerical calculations on the EW corrections for the $\mathrm{q\overline{q}} \to \mathrm{ZZ}$ background process, Giampiero Passarino for his calculations of the m_{ZZ}-dependent K factor and its variations with renormalization and factorization scales, and Marco Zaro for checking the independence on m_{ZZ} of higher-order corrections in VBF processes. We also gratefully acknowledge Alessandro Ballestrero, John Campbell, Keith Ellis, Stefano Forte, Nikolas Kauer, Kirill Melnikov, and Ciaran Williams for their help in optimizing the Monte Carlo generators for this analysis.

We congratulate our colleagues in the CERN accelerator departments for the excellent performance of the LHC and thank the technical and administrative staffs at CERN and at other CMS institutes for their contributions to the success of the CMS effort. In addition, we gratefully acknowledge the computing centres and personnel of the Worldwide LHC Computing Grid for delivering so effectively the computing infrastructure essential to our analyses. Finally, we acknowledge the enduring support for the construction and operation of the LHC and the CMS detector provided by the following funding agencies: BMWF and FWF (Austria); FNRS and FWO (Belgium); CNPq, CAPES, FAPERJ, and FAPESP (Brazil); MES (Bulgaria); CERN; CAS, MoST, and NSFC (China); COLCIENCIAS (Colombia); MSES and CSF (Croatia); RPF (Cyprus); MoER, SF0690030s09 and ERDF (Estonia); Academy of Finland, MEC, and HIP (Finland); CEA and CNRS/IN2P3 (France); BMBF, DFG, and HGF (Germany); GSRT (Greece); OTKA and NIH (Hungary); DAE and DST (India); IPM (Iran); SFI (Ireland); INFN (Italy); NRF and WCU (Republic of Korea); LAS (Lithuania); MOE and UM (Malaysia); CINVESTAV, CONACYT, SEP, and UASLP-FAI (Mexico); MBIE (New Zealand); PAEC (Pakistan); MSHE and NSC (Poland); FCT (Portugal); JINR (Dubna); MON, RosAtom, RAS and RFBR (Russia); MESTD (Serbia); SEIDI and CPAN (Spain); Swiss Funding Agencies (Switzerland); NSC (Taipei); ThEPCenter, IPST, STAR and NSTDA (Thailand); TUBITAK and TAEK (Turkey); NASU and SFFR (Ukraine); STFC (United Kingdom); DOE and NSF (USA).

References

[1] ATLAS Collaboration, "Observation of a new particle in the search for the Standard Model Higgs boson with the ATLAS detector at the LHC", *Phys. Lett. B* **716** (2012) 1,

doi:10.1016/j.physletb.2012.08.020, arXiv:1207.7214.

[2] CMS Collaboration, "Observation of a new boson at a mass of 125 GeV with the CMS experiment at the LHC", *Phys. Lett. B* **716** (2012) 30, doi:10.1016/j.physletb.2012.08.021, arXiv:1207.7235.

[3] CMS Collaboration, "Observation of a new boson with mass near 125 GeV in pp collisions at $\sqrt{s} = 7$ and 8 TeV", *JHEP* **06** (2013) 081, doi:10.1007/JHEP06(2013)081, arXiv:1303.4571.

[4] CMS Collaboration, "Study of the Mass and Spin-Parity of the Higgs Boson Candidate via its Decays to Z Boson Pairs", *Phys. Rev. Lett.* **110** (2013) 081803, doi:10.1103/PhysRevLett.110.081803, arXiv:1212.6639.

[5] ATLAS Collaboration, "Measurements of Higgs boson production and couplings in diboson final states with the ATLAS detector at the LHC", *Phys. Lett. B* **726** (2013) 88, doi:10.1016/j.physletb.2013.08.010, arXiv:1307.1427.

[6] ATLAS Collaboration, "Evidence for the spin-0 nature of the Higgs boson using ATLAS data", *Phys. Lett. B* **726** (2013) 120, doi:10.1016/j.physletb.2013.08.026, arXiv:1307.1432.

[7] CMS Collaboration, "Measurement of the properties of a Higgs boson in the four-lepton final state", *Phys. Rev. D* **89** (2014) 092007, doi:10.1103/PhysRevD.89.092007, arXiv:1312.5353.

[8] LHC Higgs Cross Section Working Group, "Handbook of LHC Higgs Cross Sections: 1. Inclusive Observables", CERN Report CERN-2011-002, (2013).

[9] LHC Higgs Cross Section Working Group, "Handbook of LHC Higgs Cross Sections: 3. Higgs Properties", CERN Report CERN-2013-004, (2013).

[10] F. Caola and K. Melnikov, "Constraining the Higgs boson width with ZZ production at the LHC", *Phys. Rev. D* **88** (2013) 054024, doi:10.1103/PhysRevD.88.054024, arXiv:1307.4935.

[11] N. Kauer and G. Passarino, "Inadequacy of zero-width approximation for a light Higgs boson signal", *JHEP* **08** (2012) 116, doi:10.1007/JHEP08(2012)116, arXiv:1206.4803.

[12] N. Kauer, "Inadequacy of zero-width approximation for a light Higgs boson signal", *Mod. Phys. Lett. A* **28** (2013) 1330015, doi:10.1142/S0217732313300152, arXiv:1305.2092.

[13] J. M. Campbell, R. K. Ellis, and C. Williams, "Bounding the Higgs width at the LHC using full analytic results for $gg \to e^+e^-\mu^+\mu^-$", (2013). arXiv:1311.3589.

[14] G. Passarino, "Higgs CAT", *Eur. Phys. J. C* **74** (2014) 2866, doi:10.1140/epjc/s10052-014-2866-7, arXiv:1312.2397.

[15] G. Passarino, "Higgs Interference Effects in gg $\to$ ZZ and their Uncertainty", *JHEP* **08** (2012) 146, doi:10.1007/JHEP08(2012)146, arXiv:1206.3824.

[16] CMS Collaboration, "Search for a standard-model-like Higgs boson with a mass in the range 145 to 1000 GeV at the LHC", *Eur. Phys. J. C* **73** (2013) 2469, doi:10.1140/epjc/s10052-013-2469-8, arXiv:1304.0213.

DRAFT

[17] CMS Collaboration, "Search for the standard model Higgs boson in the $\mathrm{H} \to \mathrm{ZZ} \to 2\ell 2\nu$ channel in pp collisions at $\sqrt{s} = 7\,\mathrm{TeV}$", *JHEP* **03** (2012) 040, doi:10.1007/JHEP03(2012)040.

[18] CMS Collaboration, "The CMS experiment at the CERN LHC", *JINST* **3** (2008) S08004, doi:10.1088/1748-0221/3/08/S08004.

[19] N. Kauer, "Interference effects for $\mathrm{H} \to \mathrm{WW/ZZ} \to \ell\bar{\nu}_\ell \ell\bar{\nu}_\ell$ searches in gluon fusion at the LHC", *JHEP* **12** (2013) 082, doi:10.1007/JHEP12(2013)082, arXiv:1310.7011.

[20] J. M. Campbell and R. K. Ellis, "MCFM for the Tevatron and the LHC", *Nucl. Phys. Proc. Suppl.* **205** (2010) 10, doi:10.1016/j.nuclphysbps.2010.08.011, arXiv:1007.3492.

[21] A. D. Martin, W. J. Stirling, R. S. Thorne, and G. Watt, "Parton distributions for the LHC", *Eur. Phys. J. C* **63** (2009) 189, doi:10.1140/epjc/s10052-009-1072-5, arXiv:0901.0002.

[22] M. Bonvini et al., "Signal-background interference effects in $gg \to H \to WW$ beyond leading order", *Phys. Rev. D* **88** (2013) 034032, doi:10.1103/PhysRevD.88.034032, arXiv:1304.3053.

[23] A. Ballestrero et al., "PHANTOM: a Monte Carlo event generator for six parton final states at high energy colliders", *Comput. Phys. Commun.* **180** (2009) 401, doi:10.1016/j.cpc.2008.10.005, arXiv:0801.3359.

[24] S. Frixione, P. Nason, and C. Oleari, "Matching NLO QCD computations with parton shower simulations: the POWHEG method", *JHEP* **11** (2007) 070, doi:10.1088/1126-6708/2007/11/070, arXiv:0709.2092.

[25] S. Alioli, P. Nason, C. Oleari, and E. Re, "A general framework for implementing NLO calculations in shower Monte Carlo programs: the POWHEG BOX", *JHEP* **06** (2010) 043, doi:10.1007/JHEP06(2010)043, arXiv:1002.2581.

[26] E. Bagnaschi, G. Degrassi, P. Slavich, and A. Vicini, "Higgs production via gluon fusion in the POWHEG approach in the SM and in the MSSM", *JHEP* **02** (2012) 088, doi:10.1007/JHEP02(2012)088, arXiv:1111.2854.

[27] P. Nason and C. Oleari, "NLO Higgs boson production via vector-boson fusion matched with shower in POWHEG", *JHEP* **02** (2010) 037, doi:10.1007/JHEP02(2010)037, arXiv:0911.5299.

[28] Y. Gao et al., "Spin determination of single-produced resonances at hadron colliders", *Phys. Rev. D* **81** (2010) 075022, doi:10.1103/PhysRevD.81.075022, arXiv:1001.3396.

[29] S. Bolognesi et al., "On the spin and parity of a single-produced resonance at the LHC", *Phys. Rev. D* **86** (2012) 095031, doi:10.1103/PhysRevD.86.095031, arXiv:1208.4018.

[30] T. Sjöstrand, S. Mrenna, and P. Skands, "PYTHIA 6.4 physics and manual", *JHEP* **05** (2006) 026, doi:10.1088/1126-6708/2006/05/026, arXiv:hep-ph/0603175.

DRAFT

[31] T. Melia, P. Nason, R. Rontsch, and G. Zanderighi, "W^+W^-, WZ and ZZ production in the POWHEG BOX", *JHEP* **11** (2011) 078, `doi:10.1007/JHEP11(2011)078`, `arXiv:1107.5051`.

[32] A. Bierweiler, T. Kasprzik, and J. H. Kühn, "Vector-boson pair production at the LHC to $\mathcal{O}(\alpha^3)$ accuracy", *JHEP* **12** (2013) 071, `doi:10.1007/JHEP12(2013)071`, `arXiv:1305.5402`.

[33] J. Baglio, L. D. Ninh, and M. M. Weber, "Massive gauge boson pair production at LHC: a next-to-leading order story", *Phys. Rev. D* **88** (2013) 113005, `doi:10.1103/PhysRevD.88.113005`, `arXiv:1307.4331`.

[34] D. De Florian, G. Ferrera, M. Grazzini, and D. Tommasini, "Higgs boson production at the LHC: transverse momentum resummation effects in the $H \to \gamma\gamma$, $H \to WW \to \ell\nu\ell\nu$ and $H \to ZZ \to 4\ell$ decay modes", *JHEP* **06** (2012) 132, `doi:10.1007/JHEP06(2012)132`, `arXiv:1203.6321v1`.

[35] GEANT4 Collaboration, "GEANT4—a simulation toolkit", *Nucl. Instrum. Meth. A* **506** (2003) 250, `doi:10.1016/S0168-9002(03)01368-8`.

[36] J. Allison et al., "GEANT4 developments and applications", *IEEE Trans. Nucl. Sci.* **53** (2006) 270, `doi:10.1109/TNS.2006.869826`.

[37] I. Anderson et al., "Constraining anomalous HVV interactions at proton and lepton colliders", *Phys. Rev. D* **89** (2014) 035007, `doi:10.1103/PhysRevD.89.035007`, `arXiv:1309.4819`.

[38] CMS Collaboration, "Identification of b-quark jets with the CMS experiment", *JINST* **8** (2013) P04013, `doi:10.1088/1748-0221/8/04/P04013`, `arXiv:1211.4462`.

[39] M. Botje et al., "The PDF4LHC Working Group Interim Recommendations", (2011). `arXiv:1101.0538`.

[40] S. Alekhin et al., "The PDF4LHC Working Group Interim Report", (2011). `arXiv:1101.0536`.

[41] H.-L. Lai et al., "New parton distributions for collider physics", *Phys. Rev. D* **82** (2010) 074024, `doi:10.1103/PhysRevD.82.074024`, `arXiv:1007.2241`.

[42] NNPDF Collaboration, "Impact of Heavy Quark Masses on Parton Distributions and LHC Phenomenology", *Nucl. Phys. B* **849** (2011) 296, `doi:10.1016/j.nuclphysb.2011.03.021`, `arXiv:1101.1300`.

[43] J. S. Gainer et al., "Beyond Geolocating: Constraining Higher Dimensional Operators in $H \to 4\ell$ with Off-Shell Production and More", (2014). `arXiv:1403.4951`.

[44] C. Englert and M. Spannowsky, "Limitations and Opportunities of Off-Shell Coupling Measurements", (2014). `arXiv:1405.0285`.

[45] M. Ghezzi, G. Passarino, and S. Uccirati, "Bounding the Higgs Width Using Effective Field Theory", (2014). `arXiv:1405.1925`.

[46] ATLAS and CMS Collaborations, LHC Higgs Combination Group, "Procedure for the LHC Higgs boson search combination in Summer 2011", Technical Report ATL-PHYS-PUB 2011-11, CMS NOTE 2011/005, (2011).

DRAFT

[47] G. J. Feldman and R. D. Cousins, “A unified approach to the classical statistical analysis of small signals”, *Phys. Rev. D* **57** (1998) 3873, `doi:10.1103/PhysRevD.57.3873`, `arXiv:physics/9711021`.

DRAFT